The Journal of Neuroscience, July 1992, 12(7): 2464–2477

Synaptic Basis for Developmental Plasticity in a Birdsong Nucleus

Richard Mooney

Division of Biology, California Institute of Technology, Pasadena, California 91125

The development and adult production of birdsong are subserved by specialized brain nuclei, including the robust nucleus of the archistriatum (RA), and its afferents originating in the caudal nucleus of the ventral hyperstriatum (HVc) and the lateral portion of the magnocellular nucleus of the anterior neostriatum (L-MAN). An *in vitro* brain slice preparation was used to characterize the electrophysiological properties of L-MAN and HVc axonal synapses within RA and to examine how these synaptic connections change during the course of song development. Electrical stimulation of L-MAN and not HVc fibers evoked excitatory synaptic potentials from virtually all RA neurons in brain slices prepared from male and female zebra finches less than 25 d of age. These "L-MAN" EPSPs were blocked substantially by the NMDA receptor antagonist D(−)-2-amino-5-phosphonopentanoic acid (D-APV; 50–100 μM) and by hyperpolarization of the postsynaptic membrane. In contrast, when slices were prepared from male finches greater than 35 d of age, electrical stimulation of the L-MAN *and* the HVc fiber tracts evoked synaptic responses from over 70% of RA neurons. Although the L-MAN EPSPs resembled those seen in RA before day 25, the "HVc" EPSPs were relatively insensitive to D-APV, but almost completely abolished by 6-cyano-7-nitroquinoxaline-2,3-dione, a non-NMDA glutamate receptor antagonist. These experiments indicate that L-MAN and HVc axons make pharmacologically distinct synapses on the same RA neurons, and that these synapses first form at different stages during development.

A central goal of modern neurobiology is to elucidate how neural circuits mediate the acquisition and maintenance of learned behaviors. In this regard, studies of synaptic properties within functionally well-defined neural systems, particularly those that are developmentally plastic and that control the production of learned behaviors, are especially useful. The present experiments examine developmental changes in synaptic transmission within a neural circuit that controls the production of learned birdsong.

Songbirds vocally imitate songs produced by other, normally conspecific, birds. Song imitation begins when a young bird listens to and memorizes another bird's song (i.e., sensory acquisition) and is followed by sensorimotor learning, during which the bird vocally rehearses its own song and matches it to the memorized model (Immelmann, 1969). This vocal matching phenomenon depends on auditory feedback, since songbirds deafened after sensory acquisition but before sensorimotor learning develop highly abnormal songs (Konishi, 1965; Price, 1979). During development, songbirds display both sensory plasticity, evinced by their ability to learn many different acoustical patterns, and motor plasticity, in that they later vocally reproduce one or more of these patterns. In many songbird species, this plasticity is developmentally restricted, so that by adulthood, the song has become highly stable and no longer requires auditory feedback (Konishi, 1965; Price, 1979).

Song is controlled by a constellation of nuclei unique to the songbird's brain, referred to collectively as the song system. One part of the song system constitutes a direct link between the forebrain and the vocal musculature, forming a descending pathway from the caudal nucleus of the ventral hyperstriatum (HVc) to the robust nucleus of the archistriatum (RA), and from RA to the hypoglossal motoneurons controlling the syringeal muscles used in singing (Nottebohm et al., 1976; Gurney, 1981) (Fig. 1*A*). HVc and RA both function as vocal premotor areas, since bilateral lesions of either nucleus disrupt singing (Nottebohm et al., 1976), and neurons within both nuclei show heightened activity immediately before and during the utterance of individual song syllables (McCasland, 1987). Another portion of the song system connects HVc to RA indirectly, by a chain of intermediate nuclei consisting of area X of the lobus parolfactorius (X), the dorsolateral part of the medial thalamus (DLM), and the lateral portion of the magnocellular nucleus of the anterior neostriatum (L-MAN) (Okuhata and Saito, 1987; Bottjer et al., 1989) (see Fig. 1*A*). In contrast to HVc and RA, L-MAN and X can be lesioned without immediately affecting adult song production, but they must be intact during sensory acquisition and sensorimotor learning if song is to develop normally (Nottebohm et al., 1976; Bottjer et al., 1984; Sohrabji et al., 1990; Scharff and Nottebohm, 1991). The recent discovery that both X and L-MAN contain song-selective auditory neurons suggests that one function of these nuclei might be to mediate auditory feedback during sensorimotor learning (Doupe and Konishi, 1991).

RA is the site of convergence between these two functionally distinct parts of the song system, receiving afferent input from both HVc and L-MAN (Nottebohm et al., 1976, 1982; Gurney, 1981; Bottjer et al., 1989). The synapses that HVc and L-MAN make within RA are critically positioned to influence vocal output, since RA neurons project directly onto the hypoglossal motoneurons that innervate the vocal musculature (nXIIts) (see Fig. 1*A*) (Gurney, 1981; Nottebohm et al., 1982). One hypothesis is that HVc and L-MAN synapses interact within RA to

Received Sept. 19, 1991; revised Dec. 26, 1991; accepted Jan. 6, 1992.

I am especially grateful for the guidance provided by Dr. Mark Konishi, to Gene Akutagawa for technical support, and to Drs. Allison Doupe and Gilles Laurent for critical discussion of the manuscript. The work was made possible by NIH Predoctoral Training Grant 5 T32 GM07737-10, the Lucille B. Markey Charitable Trust, and the McKnight Foundation.

Correspondence should be addressed to Richard Mooney, Department of Neurobiology, Stanford University School of Medicine, Stanford, CA 94305.

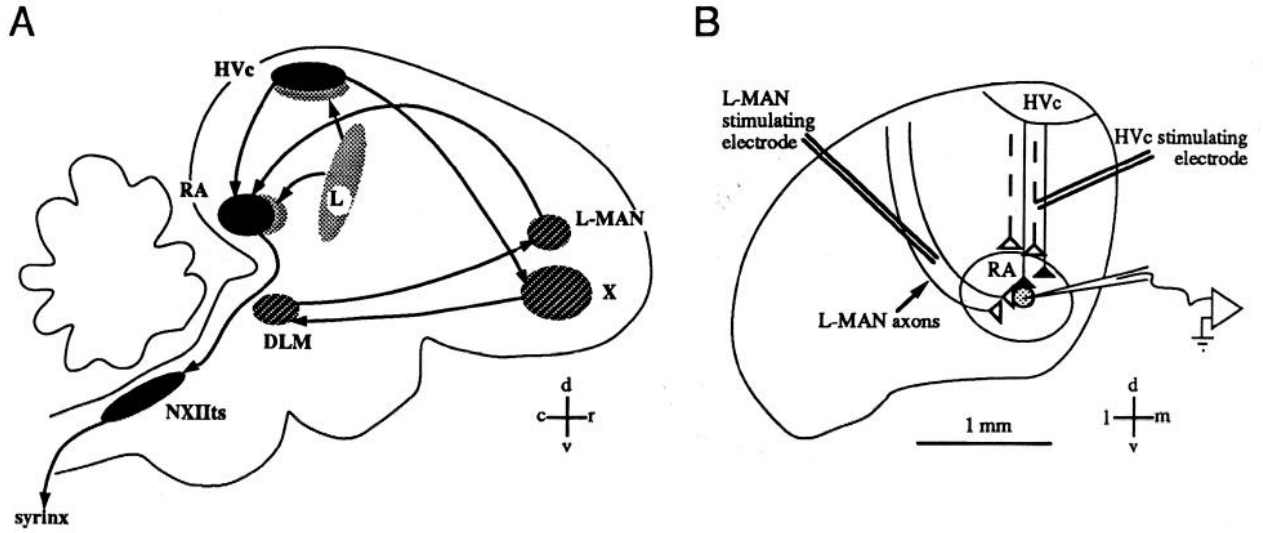

Figure 1. A schematic of the zebra finch song system and the brain slice preparation. *A,* A parasagittal view of the zebra finch brain shows the direct descending pathway from HVc to RA via the TA, and from RA onto nXIIts, in *solid black.* The indirect pathway from HVc through X, DLM, L-MAN, and back to RA is shown in *dark hatching.* Field *L,* the principal forebrain auditory area, projects to areas adjacent to HVc and RA (Kelley and Nottebohm, 1979), shown as *light shading. B,* Coronal slices of the telencephalon were made at the level of RA. *Arrow* identifies the L-MAN axon tract, and the approximate placement of the two bipolar stimulating electrodes is also indicated. Individual neurons within RA were impaled with intracellular electrodes, and electrical stimuli were applied to either L-MAN (lateral) or HVc (dorsal) fiber tracts. Slices were made either from birds less than 25 d of age, when only L-MAN terminals (shown as *white*) were present within RA, or after day 35, when terminals from both afferents were present within the nucleus. *Broken lines* with *open terminals* depict the location of HVc terminals before day 25; *solid lines* with *black terminals* depict their location after day 35.

alter the bird's vocal output during the plastic stages of song development.

Determining the nature of such synaptic interactions depends on a detailed understanding of the cellular physiology within the song system. The present experiments use an *in vitro* preparation of the zebra finch (*Taeniopygia guttata*) forebrain to characterize the intrinsic electrophysiological properties of RA neurons and to assess how the synapses that L-MAN and HVc axons make on these neurons change between 15 and 90 d after hatching, when the zebra finch's vocal plasticity is most pronounced (Immelmann, 1969). These studies indicate that L-MAN axons form electrophysiologically detectable synapses within RA substantially earlier than do HVc axons. Ultimately, L-MAN and HVc axons innervate many of the same RA neurons but evoke synaptic potentials with distinctly different pharmacological properties. Furthermore, RA neurons possess intrinsic electrophysiological properties that are well suited for their role in the control of song production. The possible implications for song development and production are discussed.

Materials and Methods

Slice preparation and intracellular recording. The finch brain slice preparation has been described in detail previously (Mooney and Konishi, 1991). Initial experiments used parasagittal slices, prepared by blocking the brain along the sagittal midline, then gluing the medial face of each hemisphere to the stainless steel tray of a vibratome. In later experiments, coronal slices were prepared by blocking the brain transversely with a razor blade about 5 mm rostral of the bifurcation of the midsagittal sinus, then gluing the caudal half of the brain rostral face down to the stainless steel tray of the vibratome. In either case, the tissue was immersed in ice-cold artificial cerebrospinal fluid (ACSF), individual slices were cut with the vibratome at 400 μm thickness, and then each slice was transferred with the blunt end of a Pasteur pipette to an interface chamber.

After a 1–2 hr recovery period, individual brain slices were transferred to a semisubmersion type recording chamber maintained at 35°C, perfused with ACSF at a rate of 3–5 ml/min. With parasagittal slices of forebrain prepared from birds less than 25 d old, slices containing RA were identified under transillumination, and a tungsten stimulating electrode was placed in the region between HVc and RA known as the tractus archistriatalis (TA). In many cases, electrical stimulation in the TA evoked synaptic responses from RA neurons, as long as the slice also contained tissue lateral to RA. Despite the possibility that electrical stimulation in the TA might excite axons arising either from L-MAN or HVc, previous anatomical studies showed that L-MAN but not HVc terminals were present within RA before day 25 (Mooney and Rao, 1987).

Further anatomical reconstruction showed that L-MAN and HVc axons describe different paths to reach RA (R. Mooney, unpublished observations; see also Bottjer et al., 1989). Although L-MAN and HVc fibers run roughly parallel to each other, in dorsoventral trajectories toward RA, and thus might be included in the same parasagittal slice, L-MAN fibers are displaced laterally to those arising from HVc. Ultimately, L-MAN axons turn and enter RA along its lateral face, whereas HVc axons, being more medially situated, enter RA along its dorsal edge (see Fig. 1*B*). Given this anatomical organization, coronal slices containing RA were prepared in which the L-MAN and HVc fiber tracts could be electrically stimulated independently of one another. Therefore, all subsequent experiments used coronal slices, and bipolar tungsten stimulating electrodes were placed $\leq$1.0 mm lateral and dorsal to nucleus RA, in areas containing respectively either the L-MAN or HVc axon tracts entering the nucleus (see Fig. 1*B*). Electrical stimulation of each fiber tract was accomplished by applying brief voltages (0.5–20 V), 100 μsec in duration, at a frequency of 0.1–100 Hz, across the two poles of either stimulus electrode.

Drugs were applied to the slice by switching between various bathing solutions via a solenoid-operated valve assembly, or via a pressure-driven puffer pipette. The pipette, which was prepared from 1 mm capillary glass and drawn to a final tip diameter of 10–100 μm, was positioned within 300 μm of the recording site. Drugs of choice were dissolved in ACSF at known concentrations and then loaded into the pipette. With this method, drug concentrations refer to the pipette solution. The actual bath concentrations were assumed to be substantially lower than the upper limit set by the pipette concentration. D(−)-2-Amino-5-phosphonopentanoic acid (D-APV) and 6-cyano-7-nitroquinoxaline-2,3 dione (CNQX) were purchased from Tocris Neuramin. QX-314 (gift of Dr. Henry Lester), a quaternary derivative of lidocaine,

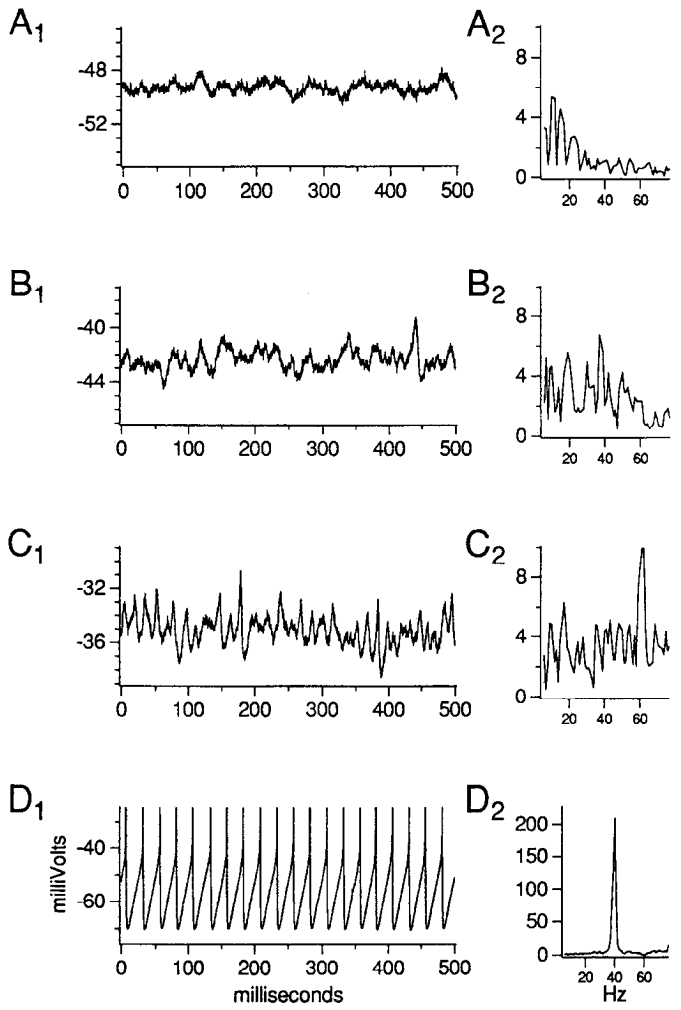

Figure 2. Subthreshold membrane potential oscillations recorded from an RA neuron. A_1–C_1 illustrate the fluctuations in membrane potential common to RA neurons *in vitro*. A_1 was recorded at the cell's actual resting potential. B_1–D_1 were obtained at increasingly more positive potentials by injecting positive currents through the recording electrode. In D_1, the membrane potential was depolarized above spike threshold, resulting in a highly regular train of action potentials (note that the vertical scale for both the raw data and the FFT in D differs from A–C; spikes are truncated in D_1). A_2–D_2 are the respective FFTs of the raw data; the *abscissa* corresponds to frequency plotted in 20 Hz intervals; the *ordinate* specifies power in arbitrary units.

was dissolved in 2 M potassium acetate at a final concentration of 75 mM. All other drugs were purchased from Sigma.

Intracellular recordings were obtained by impaling RA neurons with 50–150 MΩ electrodes filled with 3 M potassium acetate. The postsynaptic membrane potential was monitored with an intracellular amplifier, and individual events were stored on videocassette recorder in a pulse code format. To silence action potentials in those RA neurons that were spontaneously active, the postsynaptic membrane potential was subjected to DC hyperpolarization by tonically passing negative currents through the recording electrode. All signals were low pass filtered at 5 kHz, digitized at 10 kHz, and analyzed off line with synaptic potential analysis software written by Larry Proctor (Caltech) for a MASSCOMP graphics workstation. Software for performing fast Fourier transforms (FFTs) was supplied by James Mazer (Caltech). Synaptic potentials are the averages of 6–16 individual traces, unless otherwise specified. EPSP amplitudes were calculated as the maximum positive deflection from baseline and are reported as the mean ± SEM. A paired t test was used for statistical comparisons of the non-normalized EPSP amplitudes. Measurements of the EPSP slope were calculated over the first millisecond of the EPSP, starting from the EPSP onset. Statistical comparisons of the EPSPs' peak latency and onset slope (non-normalized; mean ± SEM) were made with an unpaired, two-tailed t test. The firing frequency (in Hz) was calculated as twice the total number of spikes observed over the duration of the 500 msec current pulse, as the firing rate exhibited little or no adaptation within the range of currents applied. The cell's resting potential was calculated as the difference between the observed potential immediately before and after withdrawal of the recording electrode from the cell.

Results

Intrinsic properties of RA neurons

RA neurons were characterized by high levels of spontaneous activity *in vitro*. RA neurons in slices prepared from finches of all ages displayed spontaneous subthreshold oscillations of the membrane potential, and fired highly regular trains of action potentials both spontaneously and upon depolarization. The following three sections describe these properties for male birds ranging in age from 25 to 100 d [47.4 ± 21.1 d (mean ± SD); $n = 10$].

Subthreshold properties. Subthreshold oscillations of the membrane potential often occurred spontaneously, as seen in Figure $2A_1$, but were also elicited when depolarizing currents were injected into the cell through the recording electrode (see Figs. $2B_1$,C_1; 3). FFTs of these oscillations displayed a dominant oscillatory component that increased in both frequency and amplitude with increasing depolarization of the postsynaptic cell (Fig. $2A_2$–C_2). A continuous, regular train of action potentials was generated when tonic currents displaced the membrane potential above spike threshold (Fig. $2D_1$). The action potential frequency was markedly lower than the dominant frequency of the subthreshold oscillation observed in the same cell when just below spike threshold (compare Fig. $2C_2$,D_2).

Suprathreshold properties. RA neurons fired highly regular trains of action potentials in response to suprathreshold, depolarizing currents, as shown in Figure 3*A*. When current pulses just exceeded spike threshold (top of Fig. 3*A*), a prolonged "subthreshold" oscillation often preceded the onset of the spike train. Spike threshold was reached progressively sooner after the current pulse onset as larger depolarizing currents were injected into the cell, with a concomitant decrease in the duration of the subthreshold oscillation; these oscillations disappeared altogether with very large depolarizing currents (see middle and bottom traces of Fig. 3*A*).

The highly regular trains of action potentials showed little or no acceleration or frequency adaptation, even when the depolarizing currents were several hundred milliseconds in duration. With suprathreshold depolarizing current pulse amplitudes less than +1.0 nA, the interspike interval remained nearly constant over the duration of a 500 msec stimulus, as illustrated in Figure 3*B*. The interspike interval also remained extremely constant when the cell was tonically depolarized slightly above threshold, and did not vary even over several seconds of continuous firing.

The suprathreshold firing frequency of RA neurons approximated a linear function of the amplitude of the injected current pulse (see Fig. 3*C*). The slope of the firing frequency versus injected current (f–I) relationship averaged 63.1 + 11.4 Hz/nA (mean ± SD; $n = 12$). Although most RA neurons were tested with maximum currents less than or equal to +1 nA, several cells tested above this range failed to show any pronounced saturation in firing rate.

Pharmacological analyses of intrinsic properties. Eight repetitive-spiking RA neurons were impaled with recording elec-

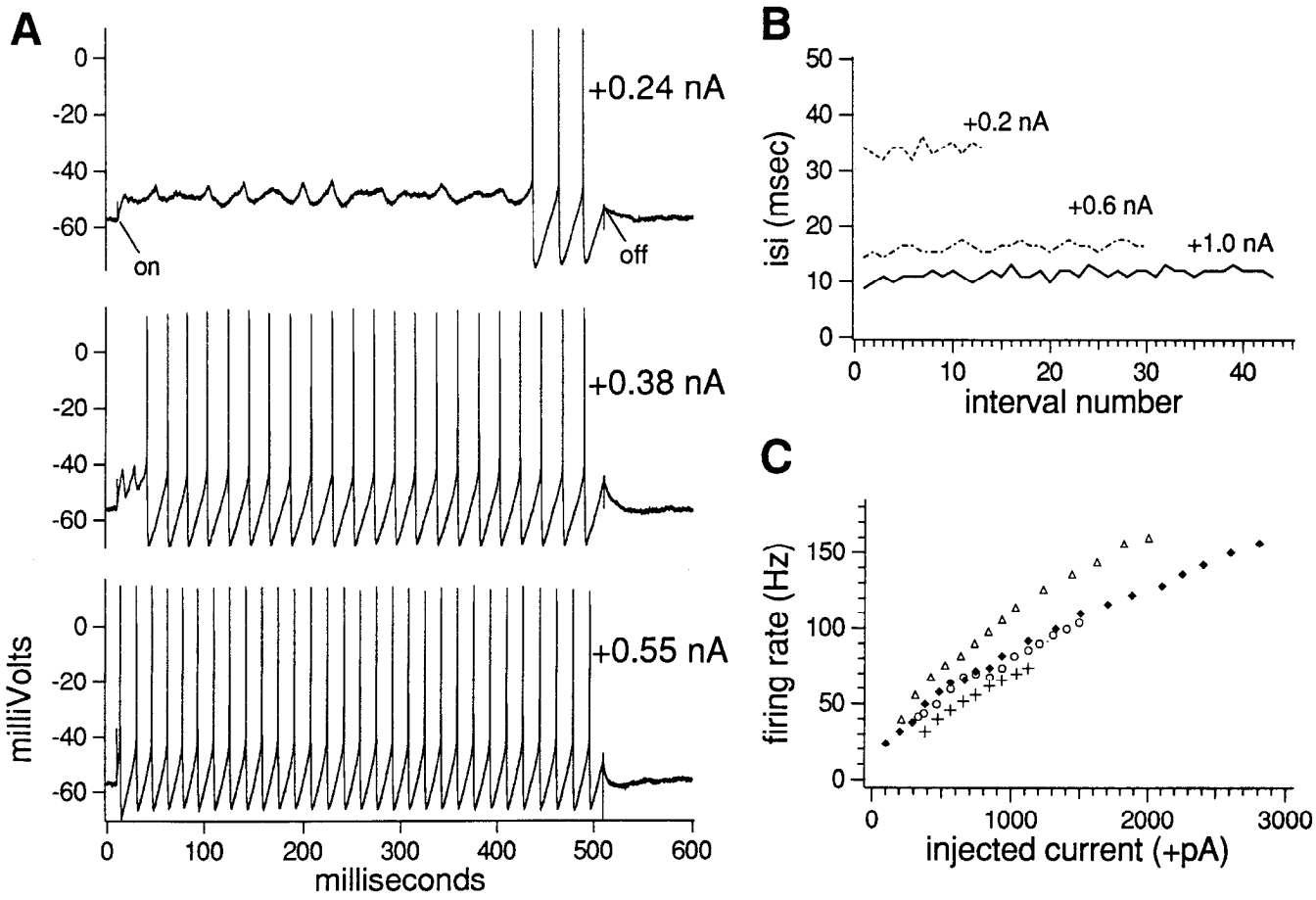

Figure 3. RA neurons fire repetitive and highly regular action potentials when injected with suprathreshold depolarizing currents. *A,* In the *top trace,* a +0.24 nA current just exceeds the spike threshold of an RA neuron. *On* and *off* mark the beginning and the end of the depolarizing current pulse. Note the prolonged subthreshold membrane potential oscillation preceding action potential onset, and the relatively high spike rate at threshold. The *middle trace* is the cell's response to a +0.38 nA current, and the *bottom trace* is its response to a +0.55 nA current. *B,* A plot of interspike interval versus the interval number demonstrates the highly regular nature of the spiking behavior recorded from RA neurons. Measurements were made over the duration of a 500-msec-long depolarization, elicited by +0.2, +0.6, and +1.0 nA currents, respectively. No pronounced accommodation was exhibited. *C,* The firing frequency plotted (in spikes/sec) as a function of the amplitude of the depolarizing current pulse. These curves typify the frequency/current (*f–I*) relationships exhibited by RA neurons.

trodes containing 75 mM QX-314 in 2 M potassium acetate. With QX-314, the regular trains of fast action potentials elicited by depolarizing currents rapidly disappeared, presumably due to the blockade of voltage-dependent sodium conductances (Strichartz, 1973). Even in the presence of QX-314, however, depolarization still evoked broader oscillations of the membrane potential (Fig. 4). The frequency of these oscillatory potentials increased directly with the amplitude of the depolarizing current pulse, as shown by FFT analysis (see Fig. $4A_2$–C_2). Noticeable damping of these potentials occurred upon more extreme depolarization (see Fig. $4A_1$–C_1). In two cells that were dialyzed with QX-314, tonic current injection also was used to elicit subthreshold oscillations. Although subthreshold oscillations were still detectable, they first became prominent at membrane potentials approximately 20 mV more positive than in control conditions.

Lowering the external calcium concentration (by bathing the slice in nominally calcium-free ACSF) affected only slightly the repetitive action potential discharge elicited by depolarizing RA neurons, when recording with 3 M potassium acetate electrodes. In both the control and low-calcium conditions, a +0.1 nA, 500-msec-long current pulse resulted in a regular train of action potentials (Fig. 5*A*). However, in the absence of any added external calcium, the spike rate was higher, and the interspike hyperpolarizing phase noticeably shallower, relative to the control response. These differences in excitability probably do not reflect the net removal of divalent cations from sites on the extracellular surface of the membrane, since the divalent cation concentration was kept constant throughout the experiment by elevating the magnesium ion concentration in the calcium-free ACSF.

The QX-314–insensitive oscillations were abolished by bathing the slice in calcium-free ACSF. Two QX-314–treated RA neurons that had displayed pronounced oscillations in response to depolarizing currents in normal ACSF were examined subsequently in the absence of external calcium (again, magnesium was supplemented to maintain the divalent concentration at a constant level throughout). The QX-314–insensitive oscillations disappeared when the control ACSF (2.4 mM calcium) was replaced with nominally calcium-free ACSF, but returned when the control ACSF was reintroduced into the recording chamber (see Fig. 5*B*).

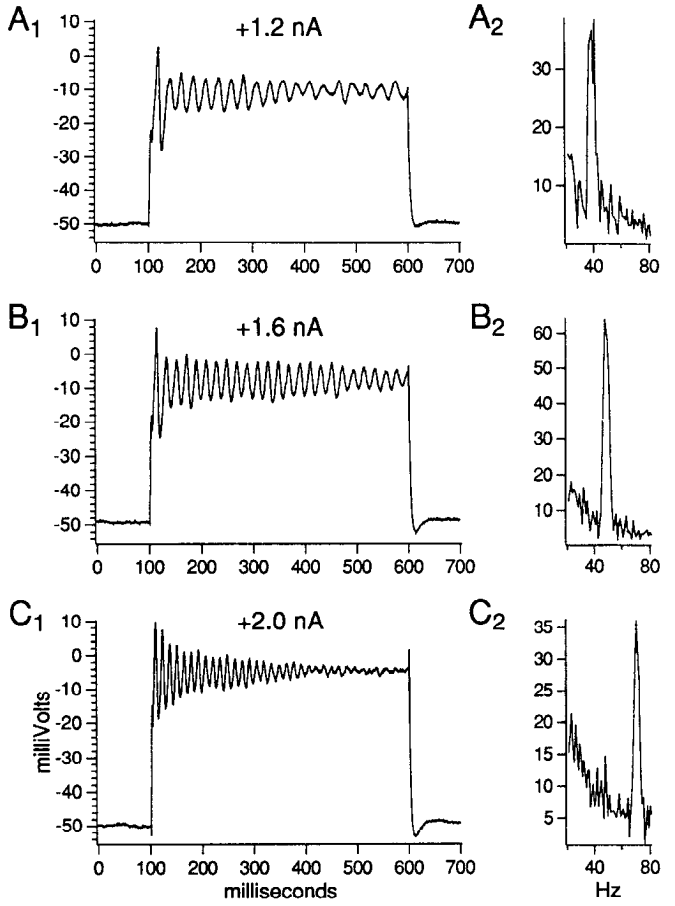

Figure 4. The membrane potential of RA neurons dialyzed with QX-314 still oscillates in response to depolarizing currents. In A_1–C_1, positive currents were injected into a QX-314–treated cell for 500 msec, beginning at $t = 100$ msec. The actual current amplitude applied in each case is listed above each trace at *top center*. In A_2–C_2, FFTs of the raw data are shown. The *ordinate* is power in arbitrary units; note that the vertical scalings in A_2–C_2 differ from each other. The peak of the FFT shifts to higher frequencies with increasing depolarization. Also note damping of the oscillation over time, especially prominent in C_1.

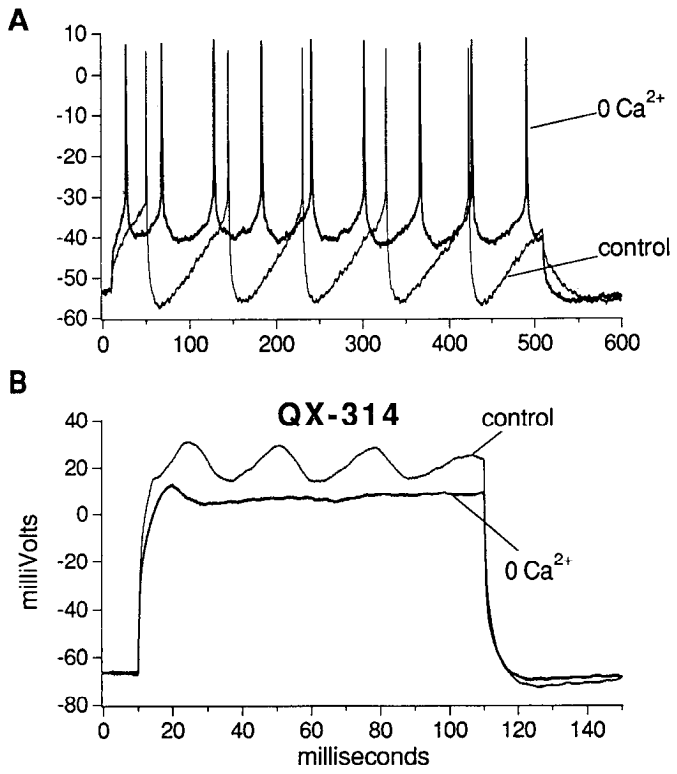

Figure 5. Lowering the external calcium ion concentration altered the excitability of RA neurons *in vitro*. *A*, An RA neuron impaled with a standard 3 M potassium acetate electrode and bathed in ACSF containing 2.4 mM external calcium and 2 mM magnesium (*control*) fired a regular train of action potentials at ~10 Hz when depolarized with a 500-msec-long, +0.1 nA current. When bathed in "calcium-free" ACSF [0 mM calcium, 4.4 mM magnesium (*0 Ca^{2+}*)], the spike rate of the same cell was nearly 20 Hz when depolarized with the same current as in the control case. Note that in the absence of any added external calcium, the interspike hyperpolarization was much less pronounced. *B*, An RA neuron impaled with a QX-314–loaded pipette exhibited an oscillating membrane potential when depolarized with a 100-msec-long, +0.8 nA current. After bathing the slice in "calcium-free" ACSF, the same depolarizing currents evoked an essentially flat response.

Synaptic transmission within nucleus RA

L-MAN versus HVc fiber stimulation before day 25. Stable intracellular recordings were obtained from a total of 88 RA neurons in coronal slices prepared from 15–25-d-old finches [22 birds comprised of 10 males and 12 females, aged 20.1 ± 2.6 d (mean ± SD); no difference in the intrinsic or synaptic properties of RA neurons was detected between male and female birds at this age]. Stimulation of the L-MAN fiber tract via the laterally positioned stimulus electrode evoked depolarizing potentials from virtually all of the RA neurons encountered in coronal slices (86 of 88 cells). These evoked potentials were classified as excitatory (EPSPs) because they could drive the cell past spike threshold. Stimulation of the HVc fiber tract, via the dorsal stimulus electrode, only evoked synaptic potentials from 12 cells, 10 of which had also responded to L-MAN fiber stimulation (10 of 88 cells), and in 2 cells that had not responded to L-MAN fiber stimulation (2 of 88 cells). Before day 25, essentially all RA neurons responded to L-MAN fiber stimulation, whereas only a small fraction responded to stimulation of the HVc fiber pathway.

Time course of the L-MAN EPSP. The potentials evoked by L-MAN fiber stimulation could be abolished by bathing the slice in very low calcium ACSF, consistent with the notion that they resulted from calcium-dependent synaptic transmission. In normal ACSF, subthreshold EPSPs evoked by L-MAN fiber stimulation had both shallow onset slopes and long rise times, but were of a fixed and relatively short latency to onset (<4 msec) (see, e.g., Figure 6*A*). In 12 RA neurons that responded only to L-MAN fiber stimulation, the stimulus-evoked EPSPs had an average onset slope of 0.89 ± 0.13 mV/msec, and attained their peak amplitudes at an average of 17.93 ± 2.13 msec after onset.

Voltage dependence of the L-MAN EPSP. The postsynaptic membrane potential strongly affected the L-MAN EPSP amplitude. Hyperpolarization of the postsynaptic membrane strongly attenuated the L-MAN EPSP amplitude (Fig. 6*A*). The EPSPs resulting from L-MAN fiber stimulation recorded from 12 RA neurons were examined at both resting and hyperpolarized membrane potentials: six of these cells were bathed in normal ACSF, five in high divalent ACSF (4 mM calcium, 4 mM magnesium), and one in very high divalent ACSF (8 mM

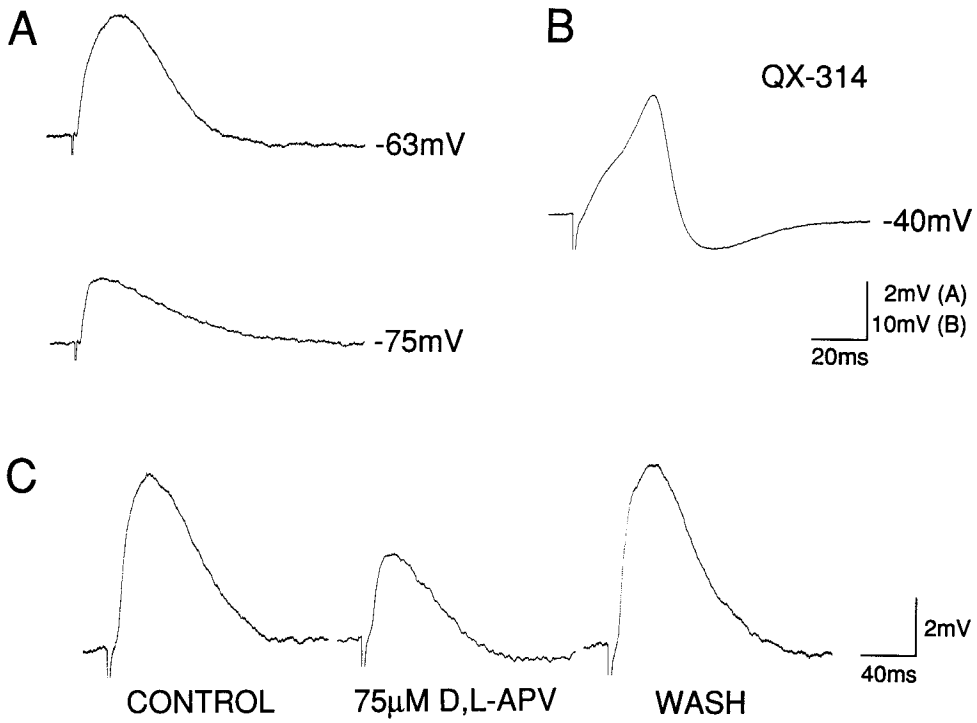

Figure 6. In brain slices prepared from birds less than 25 d of age, EPSPs evoked from RA neurons by electrically stimulating the L-MAN fiber tract could be diminished by hyperpolarizing the postsynaptic membrane and by the bath application of APV. *A,* An L-MAN EPSP evoked from an RA neuron at the actual resting potential of −63 mV, and after negative current injection had hyperpolarized the cell to −75 mV. The negative-going artifact preceding the onset of the EPSP marks the application of a brief (100 μsec) electrical stimulus to the L-MAN fiber tract. *B,* An L-MAN EPSP evoked from an RA neuron that had been dialyzed with QX-314. Between −50 and −70 mV, the EPSP behaved in a manner similar to the one shown in *A*. When positive current was used to bring the resting membrane potential to −40 mV, however, stimulation of the L-MAN fiber tract evoked an EPSP that was often crested by an all-or-none, biphasic potential. Calibration is for *A* and *B*. *C,* The bath application of 75 μM D,L-APV reversibly reduced the amplitude of the L-MAN EPSP. Resting potential was −65 mV. Recorded in high divalent ACSF (4 mM calcium, 4 mM magnesium).

calcium, 8 mM magnesium). In every condition, hyperpolarization decreased the L-MAN EPSP amplitude to between 0.36 and 0.77 of the control value (median, 0.55; $n = 12$; for each cell, the EPSP amplitude at any given membrane potential was normalized to the amplitude at the most positive membrane potential examined). In 10 of these 12 cells, hyperpolarization also reduced the EPSP's time to peak (range, 0.23–1.36 of the control value; median, 0.65; $n = 12$; normalized as above). The effects of membrane hyperpolarization on EPSP amplitude and time to peak were plotted against the range of membrane potentials actually observed in each case (Fig. 7). Note that the resting membrane potential did not reliably predict the degree to which subsequent membrane hyperpolarization actually reduced the EPSP amplitude.

In contrast to hyperpolarization, membrane depolarization augmented the L-MAN EPSP amplitude. In order that the L-MAN EPSP could be evoked at more positive potentials without activating sodium spikes, several cells were impaled with electrodes containing QX-314 to block voltage-dependent sodium channels (Strichartz, 1973). In these conditions, the EPSP continued to increase in amplitude as the postsynaptic cell was made more positive. As the membrane potential approached −40 mV, however, the EPSP occasionally triggered a broad, biphasic potential (Fig. 6*B*).

NMDA receptor antagonists block the L-MAN EPSP. The voltage dependence exhibited by the L-MAN EPSP resembled other synaptic potentials with NMDA receptor–mediated components (Thomson, 1986). To clarify the role of NMDA receptors in the genesis of the L-MAN EPSP, the NMDA receptor antagonist D-APV (Davies et al., 1981) was applied to seven RA neurons. Three were examined in zero-magnesium ACSF, one in normal ACSF, and three in high divalent ACSF. In each case, applying APV significantly reduced the amplitude of the L-MAN EPSP (see Fig. 6*C*).

In normal and high divalent ACSF, bath application of 60–75 μM D,L-APV was accompanied by a decline in the L-MAN EPSP amplitude from 4.65 ± 1.05 mV to 1.96 ± 0.49 mV ($P < 0.03$; $n = 4$, df = 3). In magnesium-free ACSF, 30 μM D-APV or 50 μM D,L-APV had an even stronger blocking effect on the L-MAN EPSP, lowering it to 0.27 ± 0.08 of the control value measured in zero-magnesium ACSF ($P < 0.001$; $n = 3$). In six of these seven cases, recordings were maintained long enough to obtain successful washouts, in which the EPSP amplitude recovered to the control value.

In three of the cells recorded in normal and high divalent ACSF, the effects of membrane hyperpolarization and APV on the L-MAN EPSP were directly compared. At more positive membrane potentials, the APV-treated EPSP was greatly diminished relative to its control counterpart. At more negative membrane potentials, however, the differences between the control and APV-treated EPSP diminished, and at the most negative potentials examined (roughly −80 to −90 mV), no differences in amplitude were apparent (not shown).

L-MAN versus HVc fiber stimulation after day 35. One hundred and ten RA neurons were recorded in brain slices prepared from male finches of 35–90 d posthatch age [36 birds, aged 48.5 ± 6.9 d (mean ± SD)]. No differences in the intrinsic or synaptic properties of RA neurons were detected within this group. These RA neurons displayed subthreshold membrane potential oscillations and responded to suprathreshold depolarization by firing regular trains of action potentials, thus resembling the RA neurons encountered in brain slices prepared from birds less than 25 d of age. Unlike their younger counterparts, however, the majority of RA neurons in slices prepared from older animals

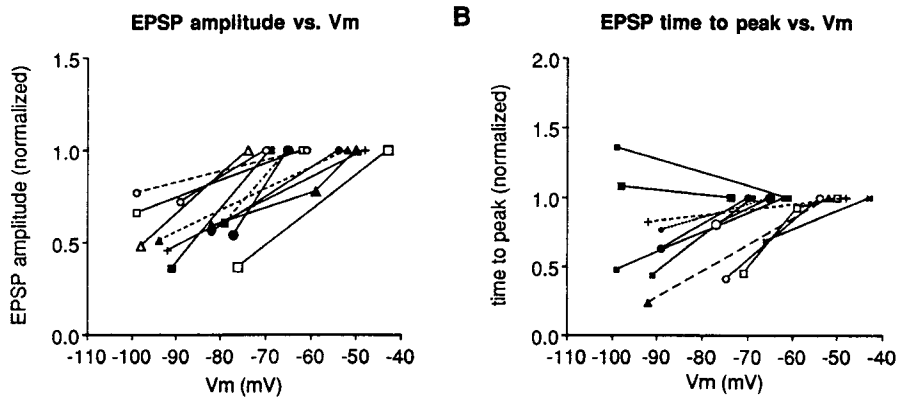

Figure 7. The postsynaptic membrane potential affected the amplitude and the time to peak of the L-MAN EPSP. *A*, The normalized EPSP amplitude plotted as a function of the membrane potential for 12 different RA neurons in slices prepared from birds less than 25 d old. Each EPSP was measured at the resting potential, then again at more negative "holding" potentials, which were obtained by passing tonic, hyperpolarizing currents through the recording electrode. EPSP amplitude was then normalized to the maximum observed value (i.e., that measured at the resting potential). *B*, The time between the onset and the peak amplitude of the EPSP is plotted as a function of the postsynaptic membrane potential. Normalization was to the value obtained at the most positive membrane potential. Ten of the 12 EPSPs exhibited a decrease in the time to reach peak amplitude as the postsynaptic membrane was made more negative.

responded to L-MAN and HVc fiber stimulation (72 of 99 cells in 30 experiments). Electrical stimulation in the L-MAN and HVc fiber tracts could evoke excitatory synaptic potentials from such "dually innervated" RA neurons (two lower amplitude traces in Fig. 8). Of the remaining RA neurons encountered, slightly more than 20% (21 of 99 cells) responded only to HVc fiber tract stimulation, and approximately 6% (6 of 99 cells) responded only to L-MAN fiber tract stimulation. In addition, eleven cells did not respond to stimulation of either the L-MAN or HVc fiber pathway.

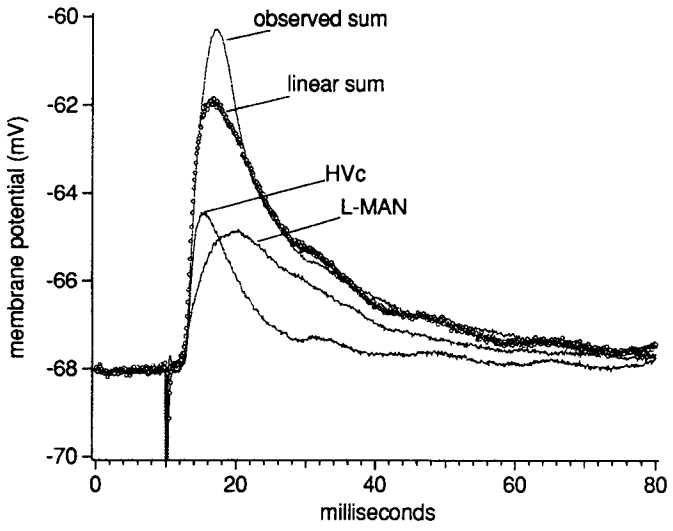

Figure 8. Electrical stimulation of both the L-MAN and HVc fiber tracts evoked EPSPs from the majority of RA neurons when slices were prepared from male finches 35 d and older. The EPSPs shown here, recorded from one such "dually innervated" RA neuron, were obtained in a brain slice made from a 50-d-old finch. L-MAN EPSPs exhibited shallower onset slopes and had longer times to peak than did HVc EPSPs. The L-MAN and HVc EPSPs summed in a nearly linear fashion when the two fiber tracts were stimulated simultaneously. The actual EPSP observed when driving the two inputs together (*observed sum*) slightly exceeded the linear sum (*open circles*) of the two EPSPs obtained when driving each input separately. Cell shown at actual resting potential; recorded in very high divalent ACSF (8 mM calcium, 8 mM magnesium). In all cases, electrical stimuli were applied at t = 10 msec.

In order to confirm that the two stimulating electrodes actually were activating different synapses on the same neuron, the EPSP recorded when the HVc and L-MAN pathways were driven together was compared to the algebraic sum of the EPSPs observed when the two inputs were driven separately. The EPSP evoked by simultaneously stimulating the two different fiber tracts closely approximated the sum of the EPSPs recorded when driving the pathways separately (see Fig. 8), consistent with the interpretation that the two stimulating electrodes activated different synapses on the same neuron.

Thirty-five RA neurons that had responded to stimulation of either one or both inputs were analyzed in greater detail. Twenty-seven of these cells responded to both L-MAN and HVc fiber stimulation. Fifteen of these dually innervated cells were treated with D-APV, eight with CNQX, two with kynurenic acid, and two by varying the membrane potential. Of the eight remaining cells, four responded to L-MAN fiber stimulation only and were tested with D-APV, and four responded to HVc fiber stimulation only, three of which were tested with D-APV and one with kynurenic acid.

Time courses of the L-MAN and HVc EPSPs. The EPSPs plotted in Figure 8 typify the recordings obtained from RA neurons responsive to both L-MAN and HVc fiber stimulation. The depolarizing potentials evoked by stimulating either input were classified as excitatory (EPSPs) because they could cause the cell to spike. The L-MAN EPSPs consistently displayed a shallower onset slope and took a longer time to reach their peak amplitude than did the HVc EPSPs, as shown in Figure 8. These differences were apparent when the L-MAN and HVc EPSPs were compared directly to one another in dually innervated RA neurons, or when the comparisons were made between cells responding to only one of the two inputs. The L-MAN EPSP onset slope averaged 1.05 ± 0.12 mV/msec (n = 28), significantly less than the value of 1.54 ± 0.12 mV/msec obtained for the HVc EPSP (n = 29; $P < 0.007$; df = 55). In the same RA neurons, the time to peak of the L-MAN EPSP, at 12.2 ± 0.81 msec (n = 28), was significantly longer than the value of 7.06

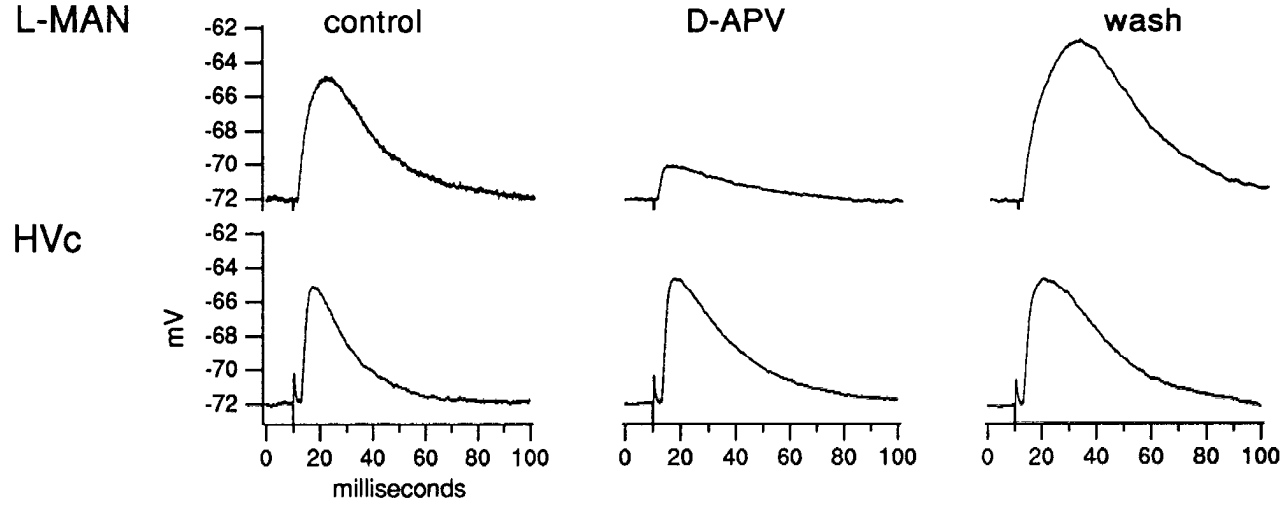

Figure 9. D-APV lowered the L-MAN EPSP amplitude without depressing the amplitude of the HVc EPSP. These EPSPs were recorded from an RA neuron that responded to electrical stimulation of both the L-MAN and HVc fiber tracts. After obtaining baseline averages (*control*), 100 μM D-APV was applied near the recording site with a puffer pipette (see Materials and Methods), and the EPSPs were again evoked by stimulating the L-MAN and HVc fiber tracts (*D-APV*). Fifteen minutes after drug application was discontinued, recovery was complete (*wash*). Recordings were made in high divalent ACSF (4 mM calcium, 4 mM magnesium). Brain slice prepared from a 40-d-old male finch.

± 0.68 msec measured for the HVc EPSP ($n = 29$; $P < 0.0001$; df = 56).

Effects of D-APV on the L-MAN and HVc EPSPs. D-APV consistently reduced the amplitude of the L-MAN EPSP but not that of the HVc EPSP (Fig. 9). This differential sensitivity to D-APV was observed in RA neurons that responded to stimulation of both the L-MAN and the HVc fiber pathways, and in those cells that responded only to stimulation of the L-MAN or HVc fiber tract. When cells that responded to one or both inputs were treated as a single group, D-APV reduced the L-MAN EPSP amplitude from 5.95 ± 0.59 mV to 2.58 ± 0.30 mV ($P < 0.0001$; $n = 19$; df = 18). Washout of the D-APV with the control ACSF was accompanied by the recovery of the L-MAN EPSP amplitude to the control level [6.27 ± 0.71 mV; $P < 0.83$; $n = 17$; df = 15 (two cells were lost before washout could be obtained)]. In contrast, D-APV did not significantly affect the HVc EPSP amplitude (4.48 ± 0.54 mV in the control vs 4.52 ± 0.60 mV in D-APV; $P < 0.87$; $n = 18$; df = 17).

Besides depressing the L-MAN EPSP amplitude, D-APV consistently reduced the actual onset slope and the time to peak of the L-MAN EPSP. In D-APV, the onset slope of the L-MAN EPSP decreased from the control value of 1.05 ± 0.12 mV/msec ($n = 28$), to 0.67 ± 0.11 mV/msec ($n = 19$) ($P < 0.03$; df = 45). D-APV also reduced the time to peak of the L-MAN EPSP from 12.2 ± 0.81 msec ($n = 29$), to 6.58 ± 0.7 msec ($n = 19$; $P < 0.0001$; df = 47). However, D-APV did not significantly affect either the HVc EPSP onset slope [1.54 ± 0.12 mV/msec in the control ($n = 29$) vs 1.29 ± 0.16 mV/msec in D-APV ($n = 18$); $P < 0.24$; df = 45] or time to peak [7.06 ± 0.68 msec in the control ($n = 29$) vs 6.30 ± 0.56 msec in D-APV ($n = 18$); $P < 0.45$; df = 45]. Note that the time to peak of the L-MAN EPSP measured in the presence of D-APV approximated the control values obtained for the HVc EPSP. Blocking NMDA receptor-mediated components of the L-MAN EPSP unmasked a faster component with a time course similar to the D-APV–resistant HVc EPSP.

In several cases, negative current injection was used to prevent the cell from firing spontaneously. To control for the possibility that the recordings were obtained at the very negative end of the current–voltage relationship of the NMDA component, the magnitude of the D-APV effect on L-MAN and HVc EPSP amplitudes was plotted against the observed membrane potential. The degree of the D-APV effect on the L-MAN or HVc EPSP amplitudes was not correlated with the postsynaptic membrane potential (not shown).

CNQX application. The HVc EPSP was blocked almost completely by CNQX, an antagonist of the quisqualate (or AMPA) subtype of glutamate receptor (Honore et al., 1988). Eight dually innervated RA neurons were treated with CNQX. In all experiments, 10 μM CNQX was applied in the immediate vicinity of the recording site with a puffer pipette. Five cells were tested in high divalent ACSF (4 mM calcium, 4 mM magnesium), two in very high divalent ACSF (8 mM calcium, 8 mM magnesium), and one in very high divalent ACSF with 10 μM bicuculline methiodide. In all conditions, CNQX greatly attenuated the HVc EPSP, while reducing the L-MAN EPSP only slightly or not at all (Fig. 10*A*). In these eight neurons, CNQX treatment reduced the HVc EPSP amplitude from 5.18 ± 0.75 mV to 1.37 ± 0.23 mV ($P < 0.0003$; $n = 8$; df = 7). The HVc EPSP amplitude recovered to 4.3 ± 0.88 mV in the six of eight cells where a partial or complete washout was accomplished, a value that did not differ significantly from the control values ($P < 0.06$; $n = 6$; df = 5). For the same RA neurons, the L-MAN EPSP amplitude measured in the presence of CNQX (4.88 ± 0.79 mV) did not differ significantly from that observed in the control conditions (5.50 ± 1.05 mV; $P < 0.37$; $n = 8$; df = 7).

The onset slope, but not the time to peak, of the HVc EPSP also was reduced significantly by CNQX treatment. The slope decreased from the control rate of 1.54 ± 0.12 mV/msec ($n = 29$) to 0.44 ± 0.04 mV/msec ($n = 8$) in the presence of CNQX ($P < 0.0001$; df = 35). Although the time to peak appeared to increase slightly in CNQX, to 8.76 ± 1.36 msec ($n = 8$), this did not differ from the control values ($P < 0.26$; df = 35). In contrast, CNQX had no significant effect on the L-MAN EPSP onset slope (0.76 ± 0.17 mV/msec; $P < 0.23$; $n = 8$; df = 34) or time to peak (11.46 ± 1.61 msec; $P < 0.67$; $n = 8$; df = 35).

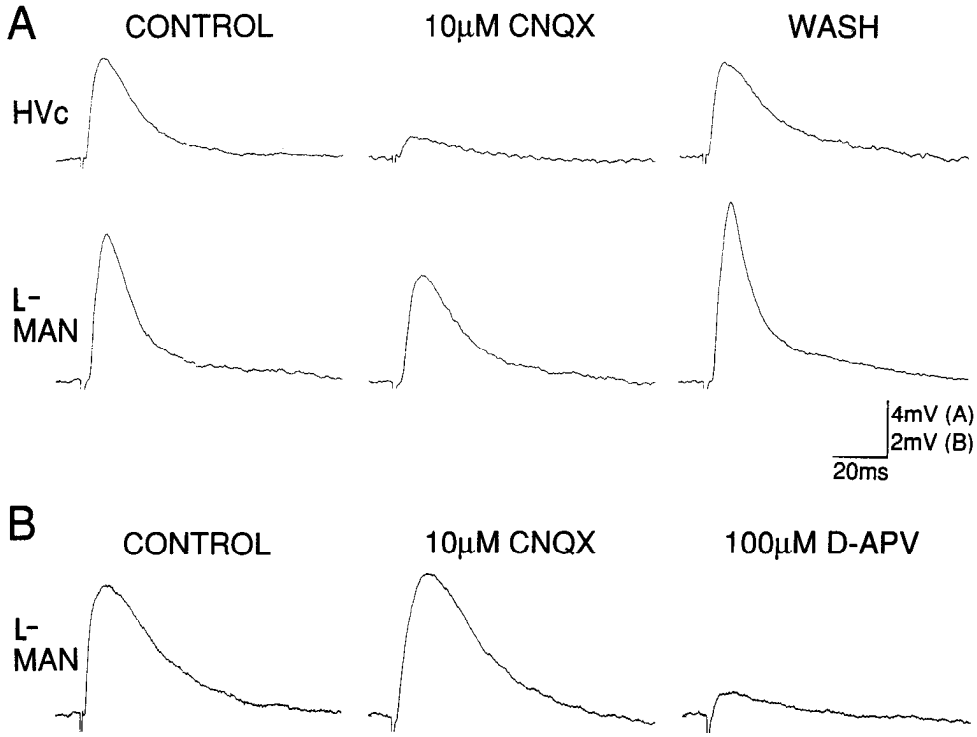

Figure 10. CNQX exerted a strong blocking effect on the HVc EPSP, without significantly affecting the L-MAN EPSP. *A*, In an RA neuron responding to stimulation of both the L-MAN and HVc fiber pathways, application of 10 μM CNQX through a puffer pipette almost completely blocked the HVc EPSP, while exerting only a slight effect on the L-MAN EPSP. Holding potential was −65 mV. *B*, Rapid, sequential application of 10 μM CNQX and 100 μM D-APV (through a puffer pipette) almost completely blocked the L-MAN EPSP in a dually innervated RA neuron. The HVc EPSP, which was almost completely abolished by CNQX, was not further reduced by D-APV (not shown).

CNQX and APV application. One dually innervated RA neuron was treated in rapid succession with 10 μM CNQX, followed by 100 μM D-APV, both applied from a puffer pipette (see Fig. 10*B*). The onset slope, but not the peak amplitude, of the L-MAN EPSP decreased upon CNQX application. The subsequent application of D-APV almost completely abolished the response, reducing the peak EPSP amplitude from 4.96 mV to 0.82 mV. These results suggest that CNQX- and D-APV-sensitive components may account for virtually all of the L-MAN EPSP. The HVc EPSP amplitude recorded from the same cell decreased from 3.12 mV to 0.74 mV, or 0.24 of the control, following CNQX application. However, the subsequent application of D-APV was not accompanied by any further reduction in the HVc EPSP amplitude (data not shown).

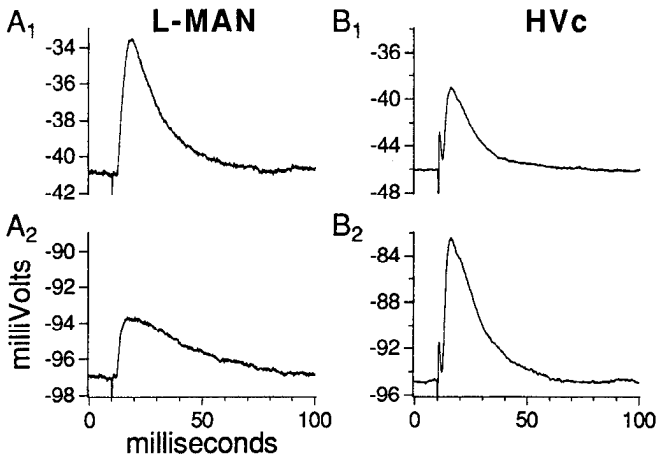

Figure 11. Altering the membrane potential of an RA neuron could exert contrasting effects on the amplitude of L-MAN and HVc EPSPs. A_1 and A_2, An L-MAN EPSP recorded from a dually innervated RA neuron was strongly attenuated as the membrane potential was varied from −41 to −97 mV. B_1 and B_2, The HVc EPSP recorded from the same cell increased substantially as the membrane potential was varied from −46 to −95 mV. Note that the L-MAN and HVc EPSPs are plotted with different vertical scaling. These traces were recorded from a neuron that was impaled with a QX-314–loaded pipette; the relatively positive and negative membrane potentials shown here were achieved by injecting tonic depolarizing or hyperpolarizing current through the recording electrode. The slice was prepared from a 35-d-old male finch and bathed in high divalent ACSF.

Kynurenic acid application. Despite the selective effects of D-APV and CNQX on the L-MAN and HVc EPSPs, kynurenic acid strongly blocked both types of input. Two dually innervated RA neurons, as well as a single RA neuron that responded only to HVc fiber stimulation, were treated with kynurenic acid (1 mM, bath application, or 10 mM, puffer pipette), a compound that acts as an antagonist at both NMDA and non-NMDA subtypes of glutamate receptors (Perkins and Stone, 1982). In these three cells, application of kynurenic acid was accompanied by a pronounced decrease in both the L-MAN and HVc EPSP amplitudes (data not shown). The L-MAN EPSP amplitude, which measured 8.32 ± 1.78 mV in the control conditions, was reduced to 2.64 ± 1.07 mV in the presence of kynurenic acid ($P < 0.08$; $n = 2$; df = 1). The HVc EPSP amplitude, which measured 7.74 ± 0.44 mV in the control conditions, was subsequently reduced to 2.10 ± 0.43 mV when kynurenic acid was present ($P < 0.001$; $n = 3$; df = 2). Considering the differential effects of D-APV and CNQX, these results suggest that L-MAN and HVc axons provide glutamatergic input onto the same RA neurons, but activate different subtypes of postsynaptic glutamate receptors.

Voltage dependence. The L-MAN and HVc EPSPs were examined at the actual resting membrane potential, as well as at more hyperpolarized potentials, which were attained by injection of tonic negative currents into the postsynaptic cell. In two dually innervated RA neurons tested in this manner, hyperpolarization of the postsynaptic cell diminished the L-MAN

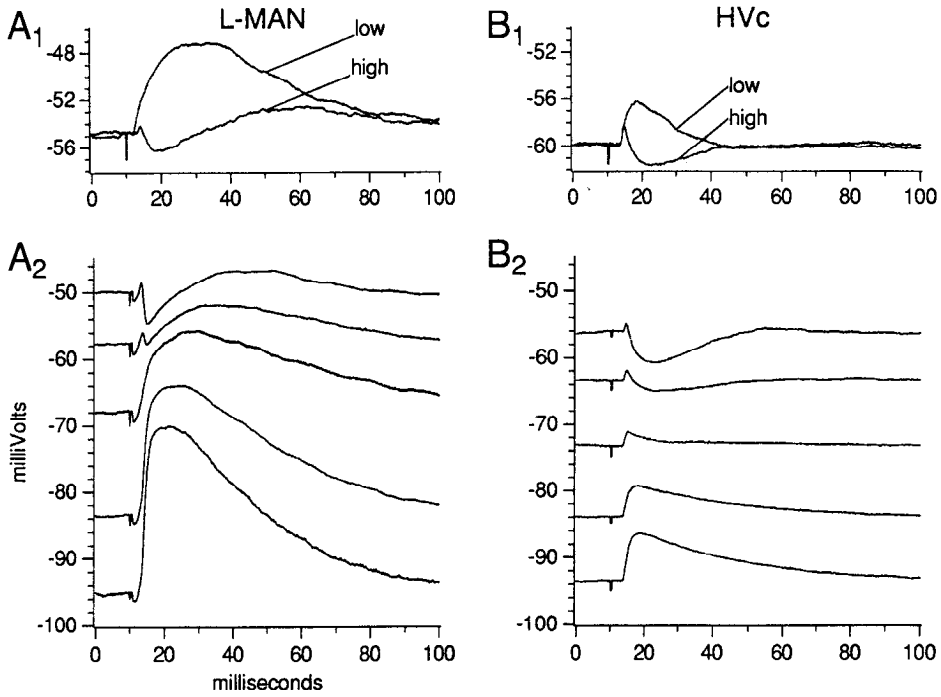

Figure 12. High-intensity electrical stimulation of the L-MAN and HVc fiber pathways often evoked polysynaptic IPSPs within RA. A_1, Low-intensity stimulation (4 V) of the L-MAN fiber pathway evoked an EPSP from an RA neuron (*low*). This response typified EPSPs evoked by L-MAN fiber stimulation, as it was attenuated by postsynaptic hyperpolarization (not shown). When a high-intensity stimulus (15 V) was then applied to the L-MAN fiber pathway, a complex potential was evoked from the same cell (*high*). A_2, Hyperpolarization of the impaled RA neuron reversed the negative-going component of the complex potential. The negative-going component inverted and became positive-going near −60 mV. Note that after reversal, the complex potential actually increased in amplitude as the membrane potential was made increasingly negative, unlike the L-MAN EPSP elicited at low intensity. B_1, A similar complex potential could also be evoked by high-intensity stimulation (3 V) of the HVc fiber pathway (*high*). Low-intensity stimulation (2.4 V) in the same cell evoked an EPSP (*low*). B_2, Hyperpolarization of the postsynaptic membrane reversed the negative-going component of the complex potential near −65 mV. After reversal, the postsynaptic potential was augmented by increasing amounts of postsynaptic hyperpolarization. All stimuli were applied at t = 10 msec.

EPSP, but augmented the HVc EPSP. In one cell, which was impaled with a pipette containing QX-314 to block sodium spikes, the membrane potential was manipulated from −40 to −95 mV, and the L-MAN EPSP decreased in amplitude, while the HVc EPSP amplitude simultaneously increased (Fig. 11). Similar results were obtained in very high divalent ACSF (8 mM calcium, 8 mM magnesium) with 10 μM bicuculline methiodide, suggesting that the voltage dependence of the HVc EPSP did not reflect contamination by reversed GABAergic IPSPs. However, it should be added that when recording from some RA neurons, the HVc EPSP was slightly attenuated by postsynaptic hyperpolarization (data not shown). Therefore, NMDA receptors might mediate a portion of the HVc EPSP, at least in some RA neurons, or perhaps at more positive membrane potentials than were achieved in the present experiments. Nonetheless, in most cases, NMDA receptors did not appear to contribute substantially to the HVc EPSP at or near normal resting membrane potentials.

Synaptic inhibition within nucleus RA. In brain slices prepared from birds of all ages, high-intensity L-MAN fiber stimulation often evoked more complex synaptic potentials from RA neurons. When an RA neuron's resting potential was more positive than −60 mV, these complex potentials were characterized by a brief, short-latency depolarizing potential, followed immediately by a hyperpolarizing component (Fig. 12A_1). The negative-going component reversed and became positive going as the postsynaptic membrane at the recording site was hyperpolarized beyond −60 mV (see Fig. 12A_2).

High-intensity stimulation of the HVc fiber tract could also evoke similar complex potentials in brain slices prepared from male birds older than 35 d. At resting potentials more positive than −60 mV, high-intensity HVc fiber stimulation often generated a brief, depolarizing potential followed by a slower, hyperpolarizing potential (see Fig. 12B_1). Typically, the negative-going portion reversed when the potential at the recording site was between −60 and −70 mV (see Fig. 12B_2).

Bicuculline methiodide (10 μM in a puffer pipette) was applied to slices in order to characterize these complex synaptic potentials. In three RA neurons tested, bicuculline blocked the hyperpolarizing component in a reversible fashion (Fig. 13*A*). In the presence of bicuculline, the initial depolarizing potential was augmented and usually exceeded spike threshold unless the stimulus intensity was reduced. The IPSP could also be abolished by treatment with either kynurenic acid or, in the case of the HVc fiber response, CNQX. Unlike bicuculline treatment, however, treatment with CNQX or kynurenic acid reduced the early, depolarizing component as well (see Fig. 13*B*).

Discussion

Intrinsic properties of RA neurons. In that RA neurons fire repetitively even over prolonged periods of depolarization, they resemble a variety of mammalian CNS neurons, including reg-

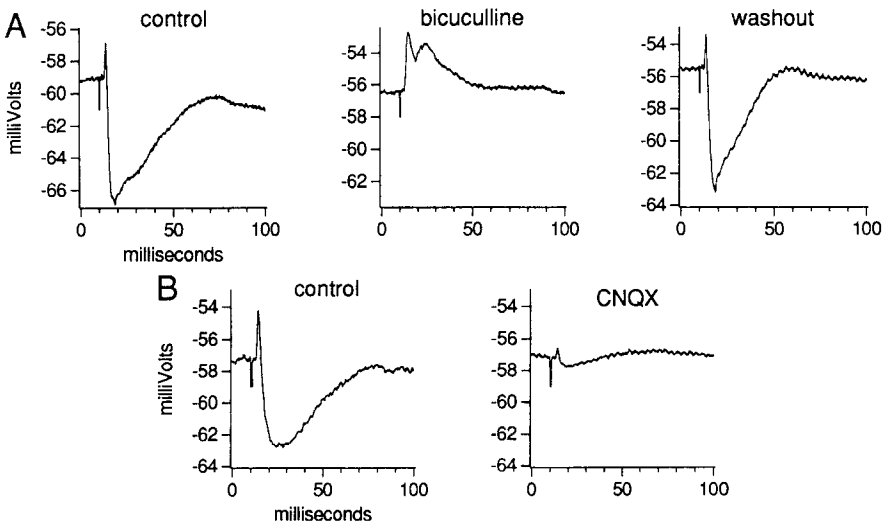

Figure 13. The pharmacology of the complex potential was consistent with a polysynaptic, $GABA_A$-mediated IPSP. *A,* The negative-going component of a complex potential evoked by HVc fiber stimulation (*control*) was almost completely blocked when 10 μM bicuculline methiodide was applied through a puffer pipette positioned near the recording electrode (*bicuculline*). Note that the positive-going component remained, however. Washout with bicuculline-free ACSF restored the complex potential to its control state. *B,* In a different cell, CNQX application (10 μM applied through a puffer pipette) almost completely blocked both parts of a complex potential. Both cells were recorded from RA neurons in a slice prepared from a 45-d-old male finch. Cells shown at actual resting potentials. Electrical stimulation was at $t = 10$ msec in all cases.

ular-spiking neocortical neurons (McCormick et al., 1985), layer V neocortical neurons (Stafstrom et al., 1984), and spinal motoneurons (Jodkowski et al., 1988). The slope of the firing frequency versus injected current (*f–I*) relationship for RA neurons fell within a range described for neocortical neurons firing in steady state (Mason and Larkman, 1990), and was about 10-fold higher than the value estimated for some spinal motoneurons (Kernell, 1965; Jodkowski et al., 1988), possibly reflecting differences in input impedance. Unlike either of these cell types, however, RA neurons *in vitro* did not exhibit any pronounced frequency adaptation even when depolarized for several hundred milliseconds.

Several ionic conductances appear to contribute to the highly regular spiking patterns of RA neurons observed *in vitro.* RA neurons treated with QX-314 did not fire fast action potentials when depolarized, but still generated slower oscillatory potentials. Lowering the external calcium ion concentration caused the QX-314–insensitive oscillations to disappear, suggesting that calcium ions are essential to this behavior. Turtle cochlear hair cells produce oscillatory membrane potentials in response to depolarization that superficially resemble the QX-314–insensitive oscillations seen within RA (Crawford and Fettiplace, 1981). A similar electrical resonance displayed by hair cells of the amphibian inner ear is due to alternating depolarizing and hyperpolarizing currents produced by voltage-dependent calcium channels and calcium-dependent potassium channels (Hudspeth and Lewis, 1988). In RA, it is tempting to speculate that similar conductances interact to produce both the subthreshold and QX-314–insensitive oscillations. These conductances could function to decrease the firing rate near spike threshold by increasing the interspike hyperpolarization. Consistent with this hypothesis, RA neurons depolarized with a fixed current had higher spike frequencies and shallower interspike hyperpolarizations when the external calcium concentration was lowered.

One striking feature of RA neurons was their ability to sustain subthreshold membrane potential oscillations when moderately depolarized. Both the amplitude and the frequency of these oscillations were influenced by the postsynaptic membrane potential, thus arguing against a purely synaptic mechanism. Nevertheless, it is possible that synaptic events contribute to these oscillations. Layer V pyramidal neurons in some areas of the mammalian neocortex display subthreshold membrane potential oscillations that resemble those seen within RA (Stafstrom et al., 1984). Given that previous comparisons between RA and layer V of mammalian motor cortex have been made on the basis of their similar descending anatomical projection patterns (Karten, 1969; Nottebohm et al., 1976), these electrophysiological similarities might reflect a common functional role. The repetitive firing behavior and lack of frequency adaptation within RA could function in the maintenance of syringeal muscle tone, since RA is linked by hypoglossal motoneurons to the vocal musculature. The steep but linear *f–I* relationship could make the output of an RA neuron quite sensitive to even a small fraction of its synaptic inputs, which could provide the finely graded control of syringeal muscle tension necessary during singing.

Synaptic inputs to RA before day 25. The present experiments indicate that L-MAN axons provide a major excitatory input to RA as early as 15 d after hatching, whereas HVc axons provide at best only a very weak input at this age. Although electrical stimulation of the L-MAN fiber tract always evoked EPSPs within RA at this age, HVc fiber stimulation rarely evoked EPSPs in RA before day 25. These findings are consistent with anatomical studies showing that L-MAN axons are present in RA as early as day 15, while HVc axons only innervate RA in large numbers after day 25 (Konishi and Akutagawa, 1985; Mooney and Rao, 1987; Herrmann and Arnold, 1991).

EPSPs evoked by L-MAN fiber stimulation were mediated predominantly by NMDA receptors. Hyperpolarization of the postsynaptic membrane significantly reduced the EPSP amplitude. EPSPs mediated by the NMDA subtype of glutamate receptor exhibit similar characteristics (Thomson, 1986), due to a voltage-dependent blockade by extracellular magnesium ions of the receptor-activated channel (Ascher and Nowak, 1988). The pronounced reduction of the L-MAN EPSP by postsynaptic hyperpolarization suggests that the NMDA receptors mediating this EPSP were on the impaled RA neuron and not on interneurons of a polysynaptic, excitatory pathway. NMDA receptor antagonists reduced the L-MAN EPSP to approximately the same extent as postsynaptic membrane hyperpolarization. D-APV, a selective, competitive antagonist of glutamate at the

NMDA receptor (Davies et al., 1981), reversibly blocked the L-MAN EPSP. The shallow onset slope and long rise time of the L-MAN EPSP resembled known monosynaptic NMDA receptor–mediated currents (Dale and Roberts, 1985; Forsythe and Westbrook, 1988; Hestrin et al., 1990). The slow kinetics of monosynaptic NMDA receptor–mediated potentials can often make them difficult to distinguish from polysynaptic EPSPs. However, even in conditions intended to suppress polysynaptic transmission (i.e., high divalents), D-APV still reduced the L-MAN EPSP amplitude by more than half of the control value. Before day 25, L-MAN terminals appear to mediate glutamatergic excitation within RA, with much of the synaptic current probably carried by NMDA receptor–activated channels located on the RA neurons impaled by the recording electrode.

Dual innervation of RA neurons after day 35

Electrical stimulation of both the L-MAN and HVc fiber tracts routinely produced EPSPs within RA in brain slices prepared from male finches greater than 35 d of age. A simple interpretation is that between days 25 and 35, HVc terminals enter RA and synapse on neurons already receiving synaptic input from L-MAN. Again, the present physiological analysis is consistent with anatomical descriptions of massive HVc axon ingrowth into RA that begins after day 25 (Konishi and Akutagawa, 1985; Mooney and Rao, 1987; Herrmann and Arnold, 1991). Apparently, RA neurons progress from an early stage in which their dominant extrinsic innervation is supplied by L-MAN axons, to a later stage of dual innervation by axons from L-MAN and HVc.

In those RA neurons receiving dual innervation, the summation of L-MAN and HVc EPSPs suggests that the two stimulating electrodes activated different synapses on the same neuron. Assuming that the dendrites within RA are passive, then such linear summation could mean that the L-MAN and HVc synapses are electrically isolated from each other (Rall et al., 1967), or that the magnitude of the subthreshold EPSPs evoked in this study were too small to affect the driving force at the different sites of synaptic input. If L-MAN and HVc axon terminals randomly intermix along the length of individual dendrites within the zebra finch RA, as they do in the canary (Canady et al., 1988), then they might interact in a nonlinear fashion when the dendrite is sufficiently depolarized to relieve the voltage-dependent blockade of NMDA receptors activated by L-MAN synaptic inputs.

L-MAN and HVc provide pharmacologically distinct input

The EPSPs evoked by L-MAN and HVc fiber stimulation have distinctly different physiological and pharmacological properties. The present work shows that L-MAN and HVc EPSPs differ dramatically in their sensitivity to D-APV, CNQX, and the postsynaptic membrane potential, and extends on preliminary observations of pharmacological heterogeneity between these two inputs to RA (Kubota and Saito, 1991; Mooney and Konishi, 1991). Even after D-APV had blocked much of the L-MAN EPSP, the HVc EPSP recorded from the same cell was largely unaffected. On the other hand, treatment with CNQX, an antagonist acting at glutamate receptors of the AMPA subtype (Honore et al., 1988), strongly blocked the HVc EPSP, but exerted no consistent effect on the L-MAN EPSP. The most parsimonious explanation consistent with these data is that HVc and L-MAN fiber stimulation evokes synaptic excitation in RA primarily through different subtypes of glutamate receptors.

The relatively disparate contribution of the NMDA receptor to the two EPSPs could also be explained if the dendrite was not isopotential at the sites of L-MAN and HVc synaptic input. This might occur if the L-MAN EPSP was larger in amplitude and electrotonically more distant from the recording site than was the HVc EPSP. In this case, the two EPSPs could appear to be of similar amplitudes because of their contrasting electrotonic distances from the recording site, but in reality the L-MAN EPSP would depolarize the postsynaptic membrane to much more positive potentials than would the smaller-amplitude HVc EPSP. Even if both inputs activated a similar postsynaptic complement of NMDA and non-NMDA receptors, the NMDA receptor would contribute more heavily to the L-MAN EPSP because of its nonlinear voltage dependence (Ascher and Nowak, 1988). The random intermixing of L-MAN and HVc synapses along the RA dendrite (Canady et al., 1988) argues against this interpretation, however. These issues should be more readily resolved by voltage clamping the postsynaptic cell with whole-cell patch electrodes.

The postsynaptic receptors activated within RA by either L-MAN or HVc fiber stimulation were not purely homogeneous populations. Although D-APV blocked much of the L-MAN EPSP, some faster components remained unaffected and could reflect contributions made by non-NMDA receptors. Similarly, in CNQX, stimulation of the HVc EPSP sometimes evoked a slower, small-amplitude, NMDA-like component. Such dual component EPSPs, characterized by both fast (non-NMDA) and slow (NMDA) components, typify monosynaptic transmission in many vertebrate systems (Dale and Roberts, 1985; Thomson et al., 1989). In RA, both afferents may activate mixed populations of NMDA and non-NMDA receptors, but these populations have markedly different compositions. On a given RA neuron, it thus appears that L-MAN terminals primarily activate NMDA receptors, while HVc terminals predominantly activate non-NMDA receptors.

Polysynaptic inhibition. Inhibitory potentials were also evoked within RA by electrical stimulation of the L-MAN and HVc fiber pathways. These IPSPs reversed when the somatic membrane potential was between -55 and -65 mV and were reversibly blocked by bicuculline, observations that suggest that they are chloride currents mediated by postsynaptic $GABA_A$ receptors. The IPSP could also be blocked by CNQX or kynurenic acid as well, suggesting that high-intensity stimulation of the L-MAN and HVc fiber tracts evokes these IPSPs by activating glutamatergic synapses on GABAergic interneurons within RA. Although the present experiments cannot determine whether these IPSPs are the product of feedback and/or feedforward inhibition, other experiments point to the latter mechanism. In parasagittal slices of zebra finch brain loaded with tritiated GABA, the orthodromic activation of RA neurons, achieved by applying electrical stimuli dorsal to the nucleus, could evoke an increased release of this inhibitory transmitter (Sakaguchi et al., 1987). In contrast, electrical stimulation rostral to RA, which would be expected to activate RA's projection neurons antidromically and thus presumably the feedback inhibitory networks that they are part of, did not increase the amount of GABA released (Sakaguchi et al., 1987). The extremely fast nature of the GABA-mediated IPSPs could serve to sharpen the temporal response properties of RA neurons. EPSPs within RA, which normally last several tens of milliseconds, can be reduced to only several milliseconds in duration when the IPSP is evoked. Inhibitory networks contribute sig-

nificantly to synaptic transmission within RA and almost certainly play an important role in sculpting the temporal patterns of activity in the nucleus.

NMDA receptors and vocal plasticity. The pharmacological heterogeneity of the L-MAN and HVc synaptic pathways could have a special function during song development. Lesion experiments have shown that L-MAN is of critical importance during plastic stages of song (Bottjer et al., 1984; Scharff and Nottebohm, 1991). Because RA is the only known efferent target of L-MAN, and RA is the last forebrain node in the descending motor-control pathway, it is an obvious site where L-MAN could exert an influence on vocal output. It is quite striking that two functionally distinct loops of the song control circuit, arising respectively from L-MAN and HVC, converge to form synapses on many of the same RA neurons. Since these RA neurons are only one synapse removed from the hypoglossal motoneuron pool, L-MAN and HVc synaptic inputs to RA could be critically positioned to influence vocal motor control. If the pathway from L-MAN conveys song-related auditory information, and the pathway from HVc is involved in vocal motor control, then the convergence of these two functionally distinct pathways within RA has special importance for the sensorimotor integration essential to song development.

The close coincidence of when HVc axons enter RA (Konishi and Akutagawa, 1985) and when the first stages of sensorimotor learning begin (Immelmann, 1969) suggests that the establishment of this pathway is important and perhaps obligatory for song production to occur. Presumably, one major obstacle facing HVc axons as they enter RA is the task of elaborating specific sets of synapses with postsynaptic neurons. The rambling and highly variable quality of subsong suggests that the initial HVc axonal ingrowth into RA produces largely random, or at least imprecise, synaptic connections. If the precision of HVc axonal connectivity with RA neurons does determine the acoustical quality of the bird's song, then the vocal refinement observed during sensorimotor learning could reflect the selective strengthening of specific sets of connections between HVc and RA. Perhaps the preexisting set of synaptic connections between L-MAN and RA guides the formation of HVc synapses on RA neurons. The sensorimotor phase of song learning depends on auditory feedback to provide error correction to the motor system. Recently, auditory units within L-MAN have been characterized that are highly selective for the bird's own song (Doupe and Konishi, 1991). One possibility is that during plastic song, auditory feedback from L-MAN can alter synaptic connectivity within RA (i.e., between ingrowing HVc axons and RA neurons), thus restructuring the descending vocal motor control pathway. Auditory inputs from L-MAN might selectively reinforce those "specific sets" of synapses between HVc and RA that generate vocalizations most closely matching the tutor song.

One cellular mechanism that could enable L-MAN axons to reorganize connections within RA involves the activation of NMDA receptors on RA neurons. In fact, NMDA receptor activation is fundamental to several forms of synaptic modification that occur within the vertebrate CNS (Collingridge et al., 1983; Cline et al., 1987; Scherer and Udin, 1989). In the developing *Xenopus* optic tectum, the realignment of binocular retinal maps following eye rotation can be blocked by NMDA receptor antagonists (Scherer and Udin, 1989). Furthermore, although the capacity for binocular realignment is typically limited to the first 3 months after metamorphosis, continuous infusion of NMDA allows realignment to occur even after the normal end of the critical period (Udin and Scherer, 1990). In the song system, NMDA receptor activation within RA could be a permissive factor mediating the synaptic modification underlying vocal plasticity. The finding that L-MAN lesions lead to an earlier development of stable, albeit abnormal, song in young zebra finches is consistent with this idea (Scharff and Nottebohm, 1991). In this regard, it may be especially relevant that L-MAN cell number declines steeply during the intermediate and latter stages of plastic song (Korsia and Bottjer, 1989). If this decline in cell number results in a smaller number of L-MAN axons innervating RA, activating fewer NMDA receptors on RA neurons, then the overall capacity for synaptic reorganization may be lost.

NMDA receptor activation is also essential to the synaptic modification that characterizes some forms of hippocampal long-term potentiation (Bliss and Lomo, 1973; Collingridge et al., 1983). When presynaptic terminals depolarize hippocampal CA1 neurons beyond a certain threshold, postsynaptic calcium influx through NMDA receptor–associated channels triggers a long-lasting increase in synaptic strength (Wigstrom et al., 1986; Malenka et al., 1988; Regehr and Tank, 1990). The associative nature of this process results in selective strengthening of all synaptic inputs to the cell that were active when threshold was exceeded (Barrionuevo and Brown, 1983). In the developing song system, as HVc terminals establish their first synaptic contacts with RA neurons, preexisting synapses from L-MAN could interact with them in an associative fashion. Perhaps synaptic connections between HVc and RA that generate vocalizations matching the tutor song could be selectively reinforced, if song-selective L-MAN neurons activated NMDA receptors in close proximity to the "correct" HVc synapses.

References

Ascher P, Nowak L (1988) The role of divalent cations in the *N*-methyl-D-aspartate responses of mouse central neurones in culture. J Physiol (Lond) 399:247–266.

Barrionuevo G, Brown TH (1983) Associative long-term potentiation in hippocampal slices. Proc Natl Acad Sci USA 80:7347–7351.

Bliss TVP, Lomo T (1973) Long-lasting potentiation of synaptic transmission in the dentate area of the anesthetized rabbit following stimulation of the perforant path. J Physiol (Lond) 232:331–356.

Bottjer SW, Miesner EA, Arnold AP (1984) Forebrain lesions disrupt development but not maintenance of song in passerine birds. Science 224:901–903.

Bottjer SW, Halsema KA, Brown SA, Miesner EA (1989) Axonal connections of a forebrain nucleus involved with vocal learning in zebra finches. J Comp Neurol 279:312–326.

Canady RA, Burd GD, DeVoogd TJ, Nottebohm F (1988) Effect of testosterone on input received by an identified neuron type of the canary song system: a Golgi/electron microscopy/degeneration study. J Neurosci 8:3770–3784.

Cline HT, Debski EA, Constantine-Paton M (1987) *N*-methyl-D-aspartate receptor antagonist desegregates eye-specific stripes. Proc Natl Acad Sci USA 84:4342–4345.

Collingridge GL, Kehl SJ, McLennan H (1983) Excitatory amino acids in synaptic transmission in the Schaffer collateral-commissural pathway of the rat hippocampus. J Physiol (Lond) 334:33–46.

Crawford AC, Fettiplace R (1981) An electrical tuning mechanism in turtle cochlear hair cells. J Physiol (Lond) 312:377–412.

Dale N, Roberts A (1985) Dual-component amino acid-mediated synaptic potentials: excitatory drive for swimming in *Xenopus* embryos. J Physiol (Lond) 363:35–59.

Davies J, Francis AA, Jones AW, Watkins JC (1981) 2-Amino-5-phosphonovalerate (2APV), a potent and selective antagonist of amino acid-induced and synaptic excitation. Neurosci Lett 21:77–81.

Doupe AJ, Konishi M (1991) Song-selective auditory circuits in the vocal control system of the zebra finch. Proc Natl Acad Sci USA 88: 11339–11343.

Forsythe ID, Westbrook GL (1988) Slow excitatory postsynaptic currents mediated by *N*-methyl-D-aspartate receptors on cultured mouse central neurones. J Physiol (Lond) 396:515–533.

Gurney ME (1981) Hormonal control of cell form and number in the zebra finch song system. J Neurosci 1:658–673.

Herrmann K, Arnold AP (1991) The development of afferent projections to the robust archistriatal nucleus in male zebra finches: a quantitative electron microscopic study. J Neurosci 11:2063–2074.

Hestrin S, Nicoll RA, Perkel DJ, Sah P (1990) Analysis of excitatory synaptic action in pyramidal cells using whole-cell recording from rat hippocampal slices. J Physiol (Lond) 422:203–225.

Honore T, Davies SN, Drejer J, Fletcher E, Jacobsen P, Lodge D, Nielsen FE (1988) Quinoxalinediones: potent competitive non-NMDA glutamate receptor antagonists. Science 241:701–703.

Hudspeth AJ, Lewis RS (1988) Kinetic analysis of voltage- and ion-dependent conductances in saccular hair cells of the bull frog, *Rana catesbeiana*. J Physiol (Lond) 400:237–274.

Immelmann K (1969) Song development in the zebra finch and other estrildid finches. In: Bird vocalizations (Hinde RA, ed), pp 61–74. London: Cambridge UP.

Jodkowski JS, Viana F, Dick TE, Berger AJ (1988) Repetitive firing properties of phrenic motoneurons in the cat. J Neurophysiol 60:687–702.

Karten H (1969) The organization of the avian telencephalon and some speculations on the phylogeny of the amniote telencephalon. Ann NY Acad Sci 167:164–179.

Kelley DB, Nottebohm F (1979) Projections of a telencephalic auditory nucleus—field L—in the canary. J Comp Neurol 183:455–470.

Kernell D (1965) High-frequency repetitive firing of cat lumbrosacral motoneurones stimulated by long-lasting injected currents. Acta Physiol Scand 65:74–86.

Konishi M (1965) The role of auditory feedback in the control of vocalization in the white-crowned sparrow. Z Tierpsychol 22:770–783.

Konishi M, Akutagawa E (1985) Neuronal growth, atrophy and death in a sexually dimorphic song nucleus in the zebra finch. Nature 315: 145–147.

Korsia S, Bottjer SW (1989) Developmental changes in the cellular composition of a brain nucleus involved with song learning in zebra finches. Neuron 3:451–460.

Kubota M, Saito N (1991) NMDA receptors participate differentially in two different synaptic inputs in neurons of the zebra finch robust nucleus of the archistriatum *in vitro*. Neurosci Lett 125:107–109.

Malenka R, Kauer JA, Zucker RS, Nicoll RA (1988) Postsynaptic calcium is sufficient for potentiation of hippocampal synaptic transmission. Science 242:81–84.

Mason A, Larkman A (1990) Correlations between morphology and electrophysiology of pyramidal neurons in slices of rat visual cortex. II. Electrophysiology. J Neurosci 10:1415–1428.

McCasland JS (1987) Neuronal control of bird song production. J Neurosci 7:23–39.

McCormick DA, Connors BW, Lightall JW, Prince DA (1985) Comparative electrophysiology of pyramidal and sparsely spiny stellate neurons of the neocortex. J Neurophysiol 54:782–806.

Mooney R, Konishi M (1991) Two distinct inputs to an avian song nucleus activate different glutamate receptor subtypes on individual neurons. Proc Natl Acad Sci USA 88:4075–4079.

Mooney R, Rao M (1987) Development and connectivity of sexually dimorphic song nuclei. Soc Neurosci Abstr 17:192.4.

Nottebohm F, Stokes TM, Leonard CM (1976) Central control of song in the canary, *Serinus canarius*. J Comp Neurol 165:457–486.

Nottebohm F, Kelley DB, Paton JA (1982) Connections of vocal control nuclei in the canary telencephalon. J Comp Neurol 207:344–357.

Okuhata S, Saito N (1987) Synaptic connections of thalamo-cerebral vocal control nuclei of the canary. Brain Res Bull 18:35–44.

Perkins MN, Stone TW (1982) An iontophoretic investigation of the actions of convulsant kynurenines and their interaction with the endogenous excitant quinolinic acid. Brain Res 247:184–187.

Price PH (1979) Developmental determinants of structure in zebra finch song. J Comp Physiol Psychol 93:260–277.

Rall W, Burke RE, Smith TG, Nelson PG, Frank K (1967) Dendritic location of synapses and possible mechanisms for the monosynaptic EPSP in motoneurons. J Neurophysiol 30:1169–1193.

Regehr WG, Tank DW (1990) Postsynaptic NMDA receptor-mediated calcium accumulation in hippocampal pyramidal cell dendrites. Nature 345:807–810.

Sakaguchi H, Asano M, Yamamoto K, Saito N (1987) Release of GABA from vocalization nucleus, the robust nucleus of the archistriatum of zebra finch *in vitro*. Brain Res 410:380–384.

Scharff C, Nottebohm F (1991) A comparative study of the behavioral deficits following lesions of various parts of the zebra finch song system: implications for vocal learning. J Neurosci 11:2896–2913.

Scherer WJ, Udin SB (1989) *N*-methyl-D-aspartate antagonists prevent binocular interaction maps in *Xenopus* tectum. J Neurosci 9: 3837–3843.

Sohrabji F, Nordeen EJ, Nordeen KW (1990) Selective impairment of song learning following lesions of a forebrain nucleus in the juvenile zebra finch. Behav Neurol Biol 53:51–63.

Stafstrom CE, Schwindt PC, Crill WE (1984) Repetitive firing in layer V neurons from cat neocortex *in vitro*. J Neurophysiol 52:264–277.

Strichartz GR (1973) Inhibition of sodium currents in myelinated nerve by quaternary derivatives of lidocaine. J Gen Physiol 62:37–57.

Thomson A, Girdlestone D, West DC (1989) A local circuit neocortical synapse that operates via both NMDA and non-NMDA receptors. Br J Pharmacol 96:406–408.

Thomson AM (1986) A magnesium-sensitive post-synaptic potential in rat cerebral cortex resembles neuronal responses to *N*-methylaspartate. J Physiol (Lond) 370:531–549.

Udin SB, Scherer WJ (1990) Restoration of the plasticity of binocular maps by NMDA after the critical period in *Xenopus*. Science 249: 669–672.

Wigstrom H, Gustafsson B, Huang Y-Y, Abraham WC (1986) Hippocampal long term potentiation is induced by pairing single afferent volleys with intracellularly injected depolarizing current pulses. Acta Physiol Scand 126:317–319.